University of Banja Luka I Faculty of Architecture, Civil Engineering and Geodesy
ISSN 2712-0570 I UDC 72

AGG+

2026_14(1)

AGG+ Journal for Architecture, Civil Engineering, Geodesy and Related Scientific Fields
АГГ+ часопис за архитектуру, грађевинарство, геодезију и сродне научне области

001-024 **Categorisation** I Original scientific paper
DOI I 10.61892/AGG202601002M
Paper received I 17/03/2026
Paper accepted I 26/06/2026

Snježana Milovanović*
University of Banja Luka, Faculty of Architecture, Civil Engineering and Geodesy, Bosnia and Herzegovina, snjezana.milovanovic@aggf.unibl.org, https://orcid.org/0009-0009-4489-2198

Aleksandar Borković
Graz University of Technology, Institute of Applied Mechanics, Austria; University of Banja Luka, Faculty of Architecture, Civil Engineering and Geodesy, Bosnia and Herzegovina,aleksandar.borkovic@aggf.unibl.org, https://orcid.org/0000-0002-4091-3379

Dijana Tatar
University of Banja Luka, Faculty of Architecture, Civil Engineering and Geodesy, Bosnia and Herzegovina, dijana.tatar@aggf.unibl.org, https://orcid.org/0000-0002-5286-9301

Ognjen Mijatović
University of Banja Luka, Faculty of Architecture, Civil Engineering and Geodesy, Bosnia and Herzegovina, ognjen.mijatovic@aggf.unibl.org, https://orcid.org/0000-0002-7859-1790

Isogeometric Analysis of In-Plane Free Vibrations of a Curved Timoshenko Beam

Snježana Milovanović*
University of Banja Luka, Faculty of Architecture, Civil Engineering and Geodesy, Bosnia and Herzegovina, snjezana.milovanovic@aggf.unibl.org, https://orcid.org/0009-0009-4489-2198

Aleksandar Borković
Graz University of Technology, Institute of Applied Mechanics, Austria; University of Banja Luka, Faculty of Architecture, Civil Engineering and Geodesy, Bosnia and Herzegovina,aleksandar.borkovic@aggf.unibl.org, https://orcid.org/0000-0002-4091-3379

Dijana Tatar
University of Banja Luka, Faculty of Architecture, Civil Engineering and Geodesy, Bosnia and Herzegovina, dijana.tatar@aggf.unibl.org, https://orcid.org/0000-0002-5286-9301

Ognjen Mijatović
University of Banja Luka, Faculty of Architecture, Civil Engineering and Geodesy, Bosnia and Herzegovina, ognjen.mijatovic@aggf.unibl.org, https://orcid.org/0000-0002-7859-1790

Isogeometric Analysis of In-Plane Free Vibrations of a Curved Timoshenko Beam

ABSTRACT

This paper presents an isogeometric formulation for the linear in-plane free vibration analysis of arbitrarily curved Timoshenko beams. The model is developed using curvilinear coordinates, ensuring a consistent kinematic description and accurate representation of strongly curved geometries. The beam geometry is described exactly using B-spline and NURBS basis functions within the isogeometric analysis framework, while the same functions are employed to approximate the displacement field. A detailed numerical study is conducted to evaluate the convergence characteristics and spectral accuracy of the proposed formulation. The convergence properties are examined through systematic *h*-, *p*-, and *k*-refinements. The obtained results demonstrate good convergence behavior; improved accuracy is achievable with a reduced number of degrees of freedom when higher continuity is employed. The strongly curved beam model yields greater accuracy than the standard simplified approach. The proposed formulation provides a robust and efficient framework for vibration analysis of curved beam structures. It offers a reliable basis for further extensions to more complex structural and dynamic problems.

Keywords: Timoshenko beam, arbitrarily curved beam, free vibrations, IGA, NURBS

* Corresponding author I

1. INTRODUCTION

Curved beam structures are widely used in a broad range of engineering. Accurate predictions of their vibrational behavior are therefore of primary importance. By accounting for shear deformation, the Timoshenko beam theory offers a realistic description of moderately thick beam structures. Although an extensive body of literature has been devoted to the vibration analysis of curved beams, research in this field remains active. In recent decades, isogeometric analysis (IGA) has become an effective computational method that bridges computer-aided design (CAD) and finite element analysis (FEA). Originally proposed in [1], IGA employs B-Splines and Non-Uniform Rational B-Splines (NURBS) for describing both geometry and unknown fields. This description enables exact geometric representation and offers higher-order interelement continuity, leading to improved accuracy and enhanced convergence properties compared to conventional finite elements.

The application of IGA to beam and rod theories has been extensively investigated. Early works demonstrated the advantages of B-spline-based formulations [2], [3]. For static analysis, a three-dimensional exact curved element with geometric torsion demonstrated high accuracy for rod structures [4]. A geometrically consistent formulation for the analysis of strongly curved beams was developed in [5], where the favorable properties of hpk-refinement strategies were emphasized. Furthermore, total Lagrangian formulations for geometrically nonlinear curved Timoshenko beams confirmed the benefits of NURBS-based discretization, particularly in reducing locking effects and improving accuracy per degree of freedom [6].

It has been observed that higher-order interelement continuity in NURBS-based approaches yields smaller absolute errors compared to C^0-continuous discretization. However, NURBS finite elements still may suffer from shear and membrane locking. To address this issue, several locking-free strategies have been proposed. The discrete shear gap (DSG) technique was employed in [7] to construct locking-free NURBS elements. In [8], isogeometric collocation methods were investigated for the Timoshenko beam problem, where mixed formulations yielded locking-free solutions independently of the polynomial degree. The application of isogeometric collocation techniques was later extended to spatial Timoshenko rods, again demonstrating locking-free behavior [9]. Higher-order NURBS discretizations with selective reduced integration and the $\bar{B}$-projection method were applied to straight and curved Timoshenko beams in [10]. Displacement-free and collocation-based formulations for Timoshenko beams were further developed in [11], providing efficient and locking-free alternatives to classical displacement-based methods. More recently, an EOSP approach based on the B-bar formulation was introduced in [12] to address shear and membrane locking in curved beams, and validated through static and vibration benchmark problems. Although a considerable research effort has been devoted to the development of locking-free isogeometric formulations, the investigation of locking behavior of highly slender beams and the development of suitable locking-free enhancements remain ongoing research topics.

Several studies have explored the application of isogeometric formulations to vibration analysis. Nonlinear vibration analysis of Bernoulli-Euler beams was studied in [13], where B-spline-based isogeometric elements combined with the harmonic balance method demonstrated high accuracy, and the k-method showed superior performance. The implementation of *h*-, *p*-, and *k*-refinement strategies for beams was investigated in [14], [15]. Moreover, a strongly curved beam formulation based on the Bernoulli-Euler beam theory was considered in [15]. Improved mass matrix formulations for isogeometric structural vibration analysis were proposed in [16], achieving optimal accuracy orders. Free vibration analysis of generally laminated deep curved Timoshenko beams with arbitrary curvature was developed in [17]. In-plane and out-of-plane free vibration analysis of curved Timoshenko beams was addressed in [18], where an effective scheme was proposed to avoid numerical locking and the superior accuracy of C^{p-1}-continuous NURBS elements was demonstrated. The influence of curve reparameterization on numerical spectra was examined in [19], where a transformation to a pseudo arc-length parameterization was proposed to improve potentially inappropriate initial geometric parameterizations. In [20], an IGA-based design approach was proposed for curved Timoshenko beams with smoothly varying cross-sections to optimize natural frequencies, ensuring smooth size distribution and stable convergence through a stability transformation method-based K-S aggregation constraint scheme. Applications to composite laminated beams reinforced with parabolic fibers were presented in [21]. Advanced interpolation techniques, such as spherical B-spline interpolation for Cosserat rod formulations, were recently introduced in [22], further enhancing convergence properties.

Although many studies have addressed the vibration analysis of curved Timoshenko beams, formulations applicable to different curvature levels remain of interest. In particular, constitutive relations for curved beams are often adopted from formulations developed for straight or weakly curved geometries, resulting in the use of a diagonal constitutive matrix that decouples axial, bending and shear effects [14], [18], [19], [23]. Such an approach can become inaccurate for moderately and strongly curved beams, for which a consistent derivation of the constitutive relations is required. Motivated by these shortcomings, the present work develops a geometrically consistent formulation for the free vibration analysis of planar Timoshenko beams. The theory is formulated for strongly curved beams, and appropriate modifications in the constitutive relations are introduced to derive the reduced constitutive model. The proposed approach provides accurate eigenfrequencies and excellent convergence properties. The convergence behavior is evaluated through *h*-, *p*-, and *k*-refinement strategies. In addition, the normalized numerical discrete spectra are evaluated in order to assess the quality of the computed eigenfrequencies, particularly in the higher modes. The k-method has been shown to provide more robust and accurate frequency spectra than conventional higher-order finite elements.

The paper is organized as follows. Section 2 briefly introduces the fundamental concepts of B-splines and NURBS functions. The following section presents the formulation of the planar Timoshenko beam and outlines the adopted kinematic description. The discrete formulation of the free vibration problem is then developed, followed by two representative numerical examples, and convergence studies are provided to verify the accuracy and performance of the proposed approach. Finally, the concluding remarks are summarized in the last section.

2. BASIS FUNCTIONS

This section briefly reviews the fundamental concepts of B-Splines and NURBS. A more detailed presentation of their definitions and properties can be found in [24], [25].

A B-Spline curve is defined as a linear combination of basis functions of order p. The curve is expressed in terms of control points $\mathbf{P}_i$ and corresponding basis functions $B_{i,p}$:

$$\mathbf{r}(\xi)=\sum_{i=1}^{N}B_{i,p}(\xi)\mathbf{P}_i. \tag{1}$$

The basis functions are polynomials constructed from a knot vector using the recursive Cox–de Boor algorithm, where each non-zero knot span represents a single isogeometric finite element. B-Spline basis functions are non-negative, form a partition of unity, and possess a local support property. Their continuity depends on the knot multiplicity, so if a knot has a multiplicity m, they are C^{p-m} continuous at the knots. *h*-refinement and *p*-refinement are achieved through knot insertion and order elevation, respectively, while the geometry remains preserved. A further refinement technique, known as *k*-refinement, uses the fact that knot insertion and order elevation processes do not commute, which enables achieving desired interelement continuity. Figure 1 shows a cubic B-Spline curve defined over a knot vector ξ={0, 0, 0, 0, 0.25, 0.5, 0.5, 0.75, 0.75, 0.75, 1, 1, 1, 1}. The control polygon is represented by a green line connecting the control points in a piecewise linear manner. The polygon is tangent to the curve at the first and last control points, due to the open knot vector, and also at ξ=0.5, where the curve is C^1-continuous. At the knot ξ=0.75, the curve is C^0-continuous, and the corresponding control point lies on the curve.

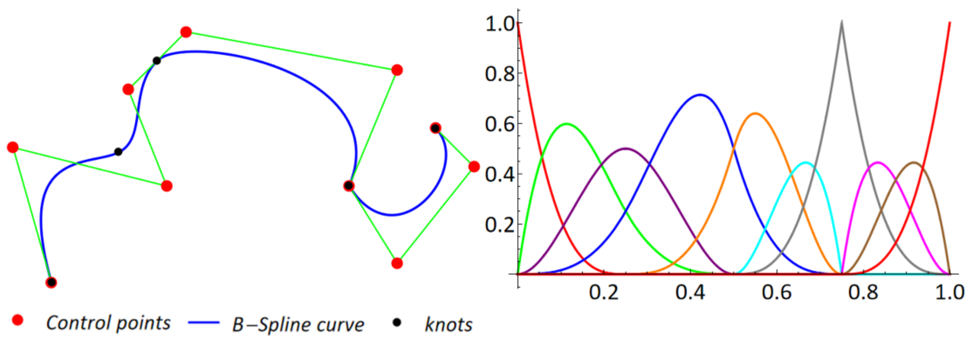

Figure 1. Cubic B-Spline curve and associated basis functions (by the authors)

In the case of rational functions, it is necessary to formulate a more general Non-Uniform Rational B-spline. NURBS curve in ℝd is obtained by a projective transformation of a B-spline curve defined in $\mathbb{R}^{d+1}$:

$$\mathbf{r}(\xi)=\sum_{i=1}^{N}R_{i,p}(\xi)\mathbf{P}_i, \quad R_{i,p}=B_{i,p}(\xi)w_i \Big/ \sum_{j=1}^{n}B_{j,p}(\xi)w_j, \tag{2}$$

where $R_{i,p}$ are rational basis functions of order p and w_i are weights associated with the i^{th} control point. All properties of the B-spline curve and its basis functions also apply to NURBS and the corresponding rational basis functions.

3. METRICS OF THE PLANE TIMOSHENKO BEAM

Unlike the classical isoparametric approach, within the IGA framework the initial geometry is described first, and then the same basis functions are employed to represent the displacement field. Many geometries can be described exactly using B-spline functions or, more generally, NURBS functions. The theory presented in this paper is derived for the plane case based on the formulation given in [26], [27]. Within this framework, a curvilinear frame of reference is adopted. It is defined by the ξ, η, and ζ coordinate axes, which correspond respectively to the beam centerline and to the principal axes of the second moment of area of the cross-section, together with the associated basis vectors $\mathbf{g}_1$, $\mathbf{g}_2$, and $\mathbf{g}_3$.

The position vector r and base vector of a beam axis $\mathbf{g}_1$ are defined as:

$$\mathbf{r} = x^m \mathbf{i}_m, \quad \mathbf{g}_1 = \mathbf{r}_{,1} = x^m_{,1} \mathbf{i}_m, \quad \mathbf{g}_1 = \frac{d\mathbf{r}}{ds}\frac{ds}{d\xi} = \sqrt{g_{11}}\mathbf{t}. \tag{3}$$

Here, $\mathbf{i}_m$ denote the unit base vectors of the global rectangular Cartesian coordinate axes x^m (m=1,2), t denotes a tangent vector, and $(\cdot)_{,1}$ represents the partial differentiation with respect to the ξ coordinate.

The relation between the parametric and arc-length coordinates of the beam axis is defined through the following expression:

$$ds^2 = dx^2 + dy^2 = (x^m_{,1})^2 d\xi^2 \rightarrow ds = \sqrt{g_{11}}\, d\xi, \qquad g_{11} = x^m_{,1} x_{m,1}. \tag{4}$$

The vector $\mathbf{g}_2$ is perpendicular to the tangential base vector and has unit length:

$$\mathbf{g}_2 = x^m_{,2} \mathbf{i}_m, \quad \mathbf{g}_2 = \Lambda \mathbf{t}, \quad \Lambda = \begin{bmatrix} 0 & 1 \\ -1 & 0 \end{bmatrix}. \tag{5}$$

The derivatives of the tangential base vector $\mathbf{g}_1$ and the base vector $\mathbf{g}_2$ with respect to the ξ coordinate are given by [26]:

$$\mathbf{g}_{1,1} = \Gamma^1_{11}\mathbf{g}_1 + \bar{K}\mathbf{g}_2, \;\; \mathbf{g}_{2,1} = -K\mathbf{g}_1. \tag{6}$$

where Γ^1_{11} is the Christoffel symbol of the second kind:

$$\Gamma^1_{11} = x^m_{,1} x_{m,11} g^{11}. \tag{7}$$

Note that K is the modulus of the curvature vector measured with respect to the Frenet-Serret frame of reference, and $\bar{K} = g_{11}K$ is the same quantity measured with respect to the parametric coordinate. Covariant and contravariant metric tensors of a beam axis are defined as follows:

$$g_{ij} = \begin{bmatrix} g_{11} & 0 \\ 0 & 1 \end{bmatrix} \rightarrow det\, g_{ij} = g_{11}, \quad g^{ij} = \begin{bmatrix} g^{11} & 0 \\ 0 & 1 \end{bmatrix} \rightarrow det\, g^{ij} = g^{11} = \frac{1}{g_{11}}. \tag{8}$$

The position vector of an arbitrary point in the reference configuration is expressed as:

$$\bar{\mathbf{r}} = \mathbf{r} + \eta \mathbf{g}_2. \tag{9}$$

The corresponding tangential base vector at an arbitrary point, together with the associated metric tensor component, is defined by:

$$\bar{\mathbf{g}}_1 = (1-\eta K)\mathbf{g}_1, \qquad \bar{g}_{11} = (1-\eta K)^2 g_{11}, \tag{10}$$

while $\bar{\mathbf{g}}_2 = \mathbf{g}_2$. According to Timoshenko beam theory, the cross-section is assumed to be rigid. However, after deformation, it no longer remains perpendicular to the beam axis. Consequently, the position of the cross-section after deformation cannot be determined solely from the kinematics of the beam axis, and it is therefore necessary to introduce the rotation of the cross-section, defined with angle φ, as an additional generalized coordinate:

$$\boldsymbol{\phi} = \varphi \mathbf{i}_3 = \varphi \mathbf{g}_3. \tag{11}$$

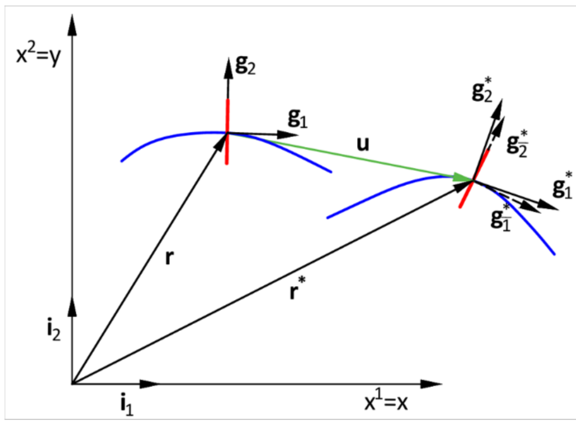

Figure 2. Kinematics of the cross section and associated base vectors (by the authors)

With **u** representing the displacement vector of the beam axis, the position vector of the beam axis in the deformed configuration is expressed as:

$$\mathbf{r}^* = \mathbf{r} + \mathbf{u}. \tag{12}$$

Figure 2 illustrates the base vectors and cross section in the undeformed and deformed configurations. The vectors $\mathbf{g}^*_{\bar{\mathrm{i}}}$ denote the base vectors after the additional rotation of the cross-section due to shear. The cross-section, shown in red, is no longer perpendicular to the beam axis. In analogy with the reference configuration, the tangential base vector of the beam axis in the deformed configuration, together with the corresponding determinant of the metric tensor, is defined as:

$$\mathbf{g}^*_1 = x^{*m}_{,1}\,\mathbf{i}_m, \qquad g^*_{11} = x^{*m}_{,1}\,x^*_{m,1}. \tag{13}$$

The modulus of the curvature of the deformed beam axis is determined as follows:

$$K^* = \frac{1}{2g_{11}}\left(\mathbf{g}^*_{\bar{1},1}\cdot\mathbf{g}^*_{\bar{2}} - \mathbf{g}^*_{\bar{2},1}\cdot\mathbf{g}^*_{\bar{1}}\right). \tag{14}$$

The derivatives of the base vectors $\mathbf{g}^*_{\bar{1}}$ and $\mathbf{g}^*_{\bar{2}}$ are given by:

$$\mathbf{g}^*_{\bar{1},1} = (\mathbf{g}_1 + \boldsymbol{\phi} \times \mathbf{g}_1)_{,1} = \mathbf{g}_{1,1} + \varphi_{,1}\mathbf{g}_3 \times \mathbf{g}_1 + \varphi\mathbf{g}_3 \times \mathbf{g}_{1,1},$$
$$\mathbf{g}^*_{\bar{2},1} = (\mathbf{g}_2 + \boldsymbol{\phi} \times \mathbf{g}_2)_{,1} = \mathbf{g}_{2,1} + \varphi_{,1}\mathbf{g}_3 \times \mathbf{g}_2 + \varphi\mathbf{g}_3 \times \mathbf{g}_{2,1}. \tag{15}$$

Using the previous relation together with relation (6) and by simplifying the resulting expression, equation (14) can be rewritten as:

$$K^* = K + \frac{1}{\sqrt{g_{11}}}\varphi_{,1}. \tag{16}$$

The component of the metric tensor in the deformed configuration within the linear analysis is obtained as:

$$g^*_{1\bar{1}} = \mathbf{g}^*_1 \cdot \mathbf{g}^*_{\bar{1}} = (\mathbf{g}_1 + \mathbf{u}_{,1}) \cdot (\mathbf{g}_1 + \varphi\sqrt{g_{11}}\mathbf{g}_2), \quad g^*_{1\bar{1}} = x^m_{,1}x_{m,1} + x^m_{,1}u_{m,1}. \tag{17}$$

The shear deformation is expressed by:

$$\gamma_{12} = \mathbf{g}^*_1 \cdot \mathbf{g}^*_{\bar{2}} = \mathbf{u}_{,1}\mathbf{g}_2 - \sqrt{g_{11}}\varphi. \tag{18}$$

Analogously to (9), the position vector of an arbitrary point in the deformed configuration is defined as:

$$\bar{\mathbf{r}}^* = \mathbf{r}^* + \eta\mathbf{g}^*_{\bar{2}}. \tag{19}$$

By differentiating the previous expression, the tangential base vector of an arbitrary point and the component of a metric tensor are obtained:

$$\bar{\mathbf{g}}^*_1 = \mathbf{g}^*_1 - \eta K^*\mathbf{g}^*_{\bar{1}}, \quad \bar{g}^*_{11} = g^*_{11} - 2\eta K^* g^*_{1\bar{1}} + \eta K^{*2}\ g_{11} \tag{20}$$

Using the relations (10) and (20), the strain at an arbitrary point of cross section is expressed as:

$$\bar{\varepsilon}_{11} = \frac{1}{2}(\bar{g}^*_{11} - \bar{g}_{11}) = \varepsilon_{11} - \eta(K^* g_{1\bar{1}} - Kg_{11}) + \frac{1}{2}\eta^2(K^{*2} - K^2)g_{11}, \tag{21}$$

where ε_{11} is the axial strain along the tangential direction at the centroid, which for the case of linear analysis reduces to:

$$\varepsilon_{11} = \frac{1}{2}(g^*_{11} - g_{11}) = x^m_{,1}u_{m,1}. \tag{22}$$

Using the expressions (16) and (17), the flexural strain is obtained as:

$$\kappa = \bar{K}^* - \bar{K} = K^* g^*_{1\bar{1}} - Kg_{11} = \sqrt{g_{11}}\varphi_{,1} + Kx^m_{,1}u_{m,1}. \tag{23}$$

In the classical beam theory, where the effects of initial curvature are often neglected, the flexural strain becomes:

$$\kappa \approx \sqrt{g_{11}}\varphi_{,1}. \tag{24}$$

Considering the Eq. (23) and the fact that the curvature change in the Frenet-Serret frame of reference is $\chi = K^* - K$, it can be written:

$$\chi = K^* - K \rightarrow \chi g_{11} = \kappa - \varepsilon_{11} K, \tag{25}$$

which leads to the final, geometrically consistent, expression for the axial strain:

$$\bar{\varepsilon}_{11} = \varepsilon_{11} - \eta\kappa + \frac{1}{2}\eta^2(\chi^2 + 2\chi K)g_{11} = g_0[(1+\eta K)\varepsilon_{11} - \eta\kappa], \quad g_0 = 1 - \eta K. \tag{26}$$

The second non-zero component of the deformation tensor at an arbitrary point is:

$$2\bar{\varepsilon}_{12} = \mathbf{g}_1^* \cdot \mathbf{g}_2^* = \gamma_{12}. \tag{27}$$

4. DISCRETE SOLUTION OF FREE VIBRATIONS

In the present paper, a linearly elastic material is considered, for which the stress at an arbitrary point is given by:

$$\bar{\sigma}^{11} = E(\bar{g}^{11})^2\bar{\varepsilon}_{11}, \quad \bar{\sigma}^{12} = 2G(\bar{g}^{11})^2\bar{\varepsilon}_{12}, \quad G = \frac{E}{2(1+\nu)}, \tag{28}$$

where G is the shear modulus. For the problem of free vibrations, the virtual work consists of an internal and an inertial part, i.e., $\delta R = \delta R_{\text{int}} + \delta R_{in}$. The internal part is evaluated using (26) and (28):

$$\delta R_{\text{int}} = \int_V [\bar{\sigma}^{11} g_0(1+\eta K)\delta\varepsilon_{11} - \bar{\sigma}^{11} g_0 \eta\delta\kappa + \bar{\sigma}^{12}\delta\gamma_{12}]dV. \tag{29}$$

Following the basic relations:

$$dV = \sqrt{\bar{g}_{11}}d\xi d\eta d\varsigma, \quad \sqrt{\bar{g}_{11}} = g_0 g_{11}, \quad \bar{g}^{11} = \frac{1}{g_0^{\,2}}g^{11}, \tag{30}$$

the internal part of virtual work is then rewritten as:

$$\delta R_{\text{int}} = \int_V (\bar{N}\delta\varepsilon_{11} - \bar{M}\delta\kappa + \bar{T}\delta\gamma_{12})dV. \tag{31}$$

Here, $\bar{N}$, $\bar{M}$ and $\bar{T}$ are the section forces energetically conjugated to the reference strains:

$$\overline{N} = E(g^{11})^2(\overline{\overline{A}}\varepsilon_{11} - \overline{I}\kappa), \quad \overline{M} = E(g^{11})^2(-\overline{I}\varepsilon_{11} - I\kappa), \quad \overline{T} = Gg^{11}\overline{A}\gamma_{12}, \tag{32}$$

with:

$$\overline{\overline{A}} = \int_A \frac{(1+\eta K)^2}{g_0} d\eta d\varsigma, \quad \overline{I} = \int_A \frac{(1+\eta K)\eta}{g_0} d\eta d\varsigma, \quad I = \int_A \frac{\eta^2}{g_0} d\eta d\varsigma, \quad \overline{A} = k\int_A \frac{1}{g_0} d\eta d\varsigma, \tag{33}$$

where k is the shear correction factor. Finally, relations (32) can be written in matrix form as:

$$\begin{bmatrix} \overline{N} \\ \overline{T} \\ \overline{M} \end{bmatrix} = \begin{bmatrix} E(g^{11})^2\overline{\overline{A}} & 0 & -E(g^{11})^2\overline{I} \\ 0 & Gg^{11}\overline{A} & 0 \\ -E(g^{11})^2\overline{I} & 0 & E(g^{11})^2 I \end{bmatrix} \begin{bmatrix} \varepsilon_{11} \\ \gamma_{12} \\ \kappa \end{bmatrix} \leftrightarrow \overline{\mathbf{R}} = \overline{\mathbf{D}}\boldsymbol{\varepsilon}. \tag{34}$$

When the off-diagonal terms of the constitutive matrix are neglected, the constitutive matrix of the reduced constitutive model becomes:

$$\overline{\mathbf{D}} \approx \begin{bmatrix} E(g^{11})^2 A & 0 & 0 \\ 0 & Gg^{11}A & 0 \\ 0 & 0 & E(g^{11})^2 I \end{bmatrix}, \tag{35}$$

where A is the area of the cross section. This classical model with reduced constitutive relations was also formulated for comparison. The dependence between the strain components and the displacement gradient, the rotation, and the rotation gradient is given as:

$$\boldsymbol{\varepsilon} = \mathbf{L}\mathbf{u}_{,1}, \quad \mathbf{L} = \begin{bmatrix} x^1_{,1} & x^2_{,1} & 0 & 0 \\ x^1_{,2} & x^2_{,2} & -\sqrt{g_{11}} & 0 \\ K\, x^1_{,1} & K\, x^2_{,1} & 0 & \sqrt{g_{11}} \end{bmatrix}, \quad \mathbf{u}_{,1} = \begin{bmatrix} u_{1,1} \\ u_{2,1} \\ \varphi \\ \varphi_{,1} \end{bmatrix}. \tag{36}$$

By introducing the vector of generalized coordinates $\mathbf{q}$, which contains degrees of freedom at control points of one element:

$$\mathbf{q}^T = [\mathbf{q}_1^T \ \mathbf{q}_2^T \ \dots \ \mathbf{q}_i^T \dots \mathbf{q}_n^T], \quad \mathbf{q}_i^T = \begin{bmatrix} u_i^1 & u_i^2 & \varphi_i \end{bmatrix}, \tag{37}$$

the following relations are derived:

$$\mathbf{u}_{,1} = \mathbf{B}\mathbf{q}, \quad \mathbf{B} = \begin{bmatrix} \mathbf{B}_1 & \mathbf{B}_2 & \dots & \mathbf{B}_i & \dots & \mathbf{B}_n \end{bmatrix}, \quad \mathbf{B}_i^T = \begin{bmatrix} R_{i,1} & 0 & 0 & 0 \\ 0 & R_{i,1} & 0 & 0 \\ 0 & 0 & R_i & R_{i,1} \end{bmatrix}. \tag{38}$$

Combining the previous relations with Eq. (36), the internal part of the virtual work can be expressed as follows:

$$\delta R_u = \int_\xi \bar{\mathbf{R}} \delta \boldsymbol{\varepsilon} \sqrt{g_{11}} d\xi = \mathbf{q}^T \int_\xi \mathbf{B}_L{}^T \bar{\mathbf{D}} \mathbf{B}_L \sqrt{g_{11}} d\xi \delta \mathbf{q} = \mathbf{q}^T \mathbf{K} \delta \mathbf{q}, \quad \mathbf{B}_L = \mathbf{L}\mathbf{B},$$
$$\mathbf{K} = \int_\xi \mathbf{B}_L{}^T \bar{\mathbf{D}} \mathbf{B}_L \sqrt{g_{11}} d\xi, \tag{39}$$

where **K** is a linear stiffness matrix of the Timoshenko beam finite element.

The inertial part of virtual work is given by:

$$\delta R_{in} = \int_\xi \ddot{\mathbf{u}}^T \mathbf{D}^M \delta \mathbf{u} \sqrt{g_{11}} d\xi, \tag{40}$$

where the displacement and acceleration vectors are defined as:

$$\mathbf{u}^{\mathrm{T}} = \begin{bmatrix} \mathbf{u}_1 & \mathbf{u}_2 & \cdots & \mathbf{u}_i & \cdots & \mathbf{u}_N \end{bmatrix}, \quad \mathbf{u}_i^{\mathrm{T}} = \begin{bmatrix} u_1 & u_2 & \varphi \end{bmatrix},$$
$$\ddot{\mathbf{u}}^{\mathrm{T}} = \begin{bmatrix} \ddot{\mathbf{u}}_1 & \ddot{\mathbf{u}}_2 & \cdots & \ddot{\mathbf{u}}_i & \cdots & \ddot{\mathbf{u}}_N \end{bmatrix}, \quad \ddot{\mathbf{u}}_i^{\mathrm{T}} = \begin{bmatrix} \ddot{u}_1 & \ddot{u}_2 & \ddot{\varphi} \end{bmatrix}. \tag{41}$$

Matrix $\mathbf{D}^M$ is given by :

$$\mathbf{D}^M = \begin{bmatrix} A^M & 0 & 0 \\ 0 & A^M & 0 \\ 0 & 0 & I^M \end{bmatrix}, \tag{42}$$

where the simple geometric cross-sectional properties are introduced:

$$A^M = \int_A g_0 \, d\eta d\zeta = \int_A d\eta d\zeta \,, \quad I^M = \int_A g_0 \, \eta^2 d\eta d\zeta = \int_A \eta^2 d\eta d\zeta \,. \tag{43}$$

The dependence of vectors given in (41) and vectors containing the degrees of freedom are defined as follows:

$$\mathbf{u}_i = \mathbf{L}_{Mi} \mathbf{q}_i \,, \; \ddot{\mathbf{u}}_i = \mathbf{L}_{Mi} \ddot{\mathbf{q}}_i \,,$$
$$\mathbf{L}_{Mi} = \begin{bmatrix} R_i & 0 & 0 \\ 0 & R_i & 0 \\ 0 & 0 & R_i \end{bmatrix}, \; \mathbf{L}_M = \begin{bmatrix} \mathbf{L}_{M1} & \mathbf{L}_{M2} & \cdots & \mathbf{L}_{Mi} & \cdots & \mathbf{L}_{MN} \end{bmatrix}. \tag{44}$$

The inertial part of virtual work is now expressed as:

$$\delta R_{in} = \ddot{\mathbf{q}}^{\mathrm{T}} \int_\xi \mathbf{L}_M^{\mathrm{T}} \mathbf{D}^M \mathbf{L}_M \sqrt{g_{11}} \, d\xi \, \delta \mathbf{q} = \ddot{\mathbf{q}}^{\mathrm{T}} \mathbf{M} \delta \mathbf{q},$$
$$\mathbf{M} = \int_\xi \mathbf{L}_M^{\mathrm{T}} \mathbf{D}^M \mathbf{L}_M \sqrt{g_{11}} \, d\xi, \tag{45}$$

where **M** is a consistent mass matrix of the Timoshenko beam finite element. Using the relations (39) and (45), the spatially discretized principle of virtual work is now defined as:

$$\mathbf{M}\ddot{\mathbf{q}}(t)+\mathbf{K}\mathbf{q}(t)=0. \tag{46}$$

By assuming synchronous and harmonic motion:

$$\mathbf{q}=\overline{\mathbf{q}}e^{i\omega t}, \tag{47}$$

the eigenvalue problem is obtained:

$$\left(\mathbf{K}-\omega^2\mathbf{M}\right)\overline{\mathbf{q}}=\mathbf{0}. \tag{48}$$

The solutions of Eq. (48) are pairs of eigenfrequencies ωn and corresponding eigenvectors $\bar{\boldsymbol{q}}_n$.

5. NUMERICAL EXAMPLES

In this section, a detailed analysis of the free vibrations of arbitrarily curved in-plane beams is carried out. Through selected numerical examples, the influence of mesh refinement techniques on the solution is investigated. Numerical integration is performed using Gauss quadrature formulas, with *p*+1 integration points. The convergence behavior was investigated using *h*-, *p*-, and *k*-refinement strategies. The resulting frequencies ω_n^h for an nth mode are normalized with respect to the reference numerical solution ω_n, which is obtained with a significantly greater number of degrees of freedom.

The objective of this study is to investigate the effect of strong curvature on the structural response of the beam. The model that employs the constitutive relation given in Eq. (34) for the evaluation of internal forces is referred to as $IGA\ \bar{D}^S$. The second model is formulated based on the decoupled constitutive approach, in which the off-diagonal terms are neglected. This constitutive relation is given in Eq. (35) and is denoted as $IGA\ \bar{D}^0$. For clarity, the differences between these formulations are summarized in Table 1.

Table 1. Differences between the models

	$IGA\ \bar{D}^S$	$IGA\ \bar{D}^0$
Constitutive matrix	Eq. (34)	Eq. (35)
Flexural strain	Eq. (23)	Eq. (24)

To compare both formulations, the analysis is performed for different values of the beam curviness measure, defined as the product of the maximum curvature and the cross-sectional height, $K_{max}h$ [15]. In addition, an isotropic two-dimensional model is constructed in Abaqus using a dense mesh of CPS3 elements (3-node linear triangular plane stress elements) in order to create a comparable reference model for strongly curved beams. The converged solutions were obtained using fine meshes consisting of more than 100 000 CPS3 elements, depending on the example. For the lowest n modes, the absolute cumulative difference $\omega_{i,ref}$ is calculated as:

$$\sum_{i=1}^{n}\left|\frac{\omega_i}{\omega_{i,ref}}-1\right|. \tag{49}$$

For higher-order NURBS discretization schemes, the locking issues are reduced in comparison with standard low-order Lagrange approximations. To further alleviate these effects, special methods are often required [10]. The locking issues are not considered in the present study and will be addressed in future research.

5.1. CIRCULAR ARC

In the first example, a quarter-circle beam with a rectangular cross-section, clamped at the left end, is analyzed. The geometry is represented using quadratic NURBS, as shown in Figure 3. The Young's modulus is E=10^6, Poisson's ratio is v=0, and the mass density is ρ=2.5. The cross-section is rectangular, with a unit width and varying height. The example provides a detailed investigation of the applicability of IGA models for different levels of Kh. The results are also compared with the analytical solutions reported in [23].

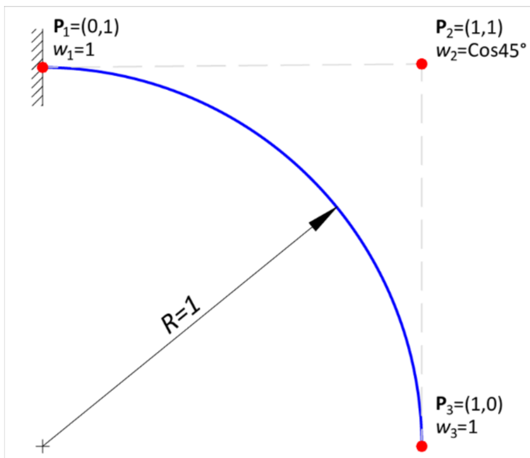

Figure 3. Circular arc (by the authors)

Table 2 and Table 3 present the natural frequencies of the first ten modes for two levels of curviness, Kh=0.2 and Kh=0.5, normalized by $r\sqrt{E/\rho}$, where r is the radius of gyration of the cross section. The results of the isogeometric analysis are obtained using a mesh consisting of 50 quartic elements with C^3 interelement continuity, corresponding to 162 degrees of freedom for the Timoshenko beam theory.

For the case Kh=0.2, the numerical solutions obtained with the model $IGA\ \bar{D}^0$ show excellent agreement with the analytical results. The results obtained with IGA models are compared with a 2D Abaqus model. The cumulative differences with respect to the Abaqus model remain very small, around 2.5%. In contrast, for the reduced constitutive model $IGA\ \bar{D}^0$, the cumulative difference increases to approximately 5.2%, indicating a slight loss of accuracy when coupling effects are neglected. The $IGA\ \bar{D}^S$ model is also compared with the results reported in [15], where a formulation for strongly curved beams considering the effects of rotatory inertia is employed. It is observed that the higher modes in [15] are not correctly captured, primarily due to the neglect of shear deformation effects.

Table 2. Comparison of the lowest ten normalized eigenfrequencies of the circular arc for Kh=0.2

Mode	$IGA\ \bar{D}^S$	$IGA\ \bar{D}^0$	[15]	Abaqus, CPS3 element	[23]
1	1.486	1.482	1.494	1.481	1.482
2	6.669	6.620	7.046	6.683	6.620
3	18.111	18.074	19.260	18.080	18.074
4	24.804	24.720	25.820	24.810	24.720
5	37.876	37.700	43.930	37.930	37.700
6	53.543	53.510	54.030	53.430	53.510
7	57.913	57.835	70.380	57.890	57.835
8	78.070	77.611	87.290	78.380	77.611
9	87.744	88.195	100.300	87.130	88.194
10	100.027	99.523	121.200	100.300	99.523

As the curviness increases to *Kh*=0.5, a different trend becomes evident. The numerical results from $IGA\ \bar{D}^0$ model again coincide very closely with the analytical solutions. When $IGA\ \bar{D}^S$ model is compared with the Abaqus model, the maximum difference occurs in the tenth mode and reaches 5.18%, with a cumulative difference of 20.56%. Comparing the $IGA\ \bar{D}^0$model with the Abaqus model, the cumulative difference increases up to 28.66%. Furthermore, comparing $IGA\ \bar{D}^S$ model with [15], the relative differences become significantly more pronounced. The differences are mainly attributed to the neglect of shear deformation effects in [15], especially for higher modes and larger curviness. This suggests that, depending on beam curviness and thickness, using an appropriate beam theory with a consistent formulation becomes essential.

Table 3. Comparison of the lowest ten normalized eigenfrequencies of the circular arc for Kh=0.5

Mode	$IGA\ \bar{D}^S$	$IGA\ \bar{D}^0$	[15]	Abaqus, CPS3 element	[23]
1	1.429	1.406	1.471	1.400	1.406
2	4.963	4.793	6.065	5.038	4.793
3	9.000	9.062	9.331	8.819	9.062
4	14.501	14.062	19.730	14.680	14.062
5	20.669	20.930	20.620	20.000	20.93
6	23.004	22.762	33.120	23.060	22.762
7	30.969	30.311	34.380	30.830	30.311
8	33.977	34.135	46.660	32.530	34.135
9	34.989	35.358	49.070	35.010	35.357
10	40.883	39.979	60.690	38.870	39.979

The convergence analysis for the curviness *Kh*=0.2 and $IGA\ \bar{D}^S$ model, performed with respect to h-refinement using cubic NURBS with C^1 and C^2 interelement continuity, is presented in Figure 4. The reference solution is computed on a mesh consisting of 120 quartic elements with C^3 interelement continuity. The orders of convergence are estimated, and the results demonstrate good convergence behavior, with higher accuracy for the lower modes and lower accuracy for the higher modes. The natural frequency of the first mode converges for each interelement continuity, even on a relatively coarse mesh. The convergence rates are close to the theoretical rate of 2*p*, and they benefit from higher interelement continuity.

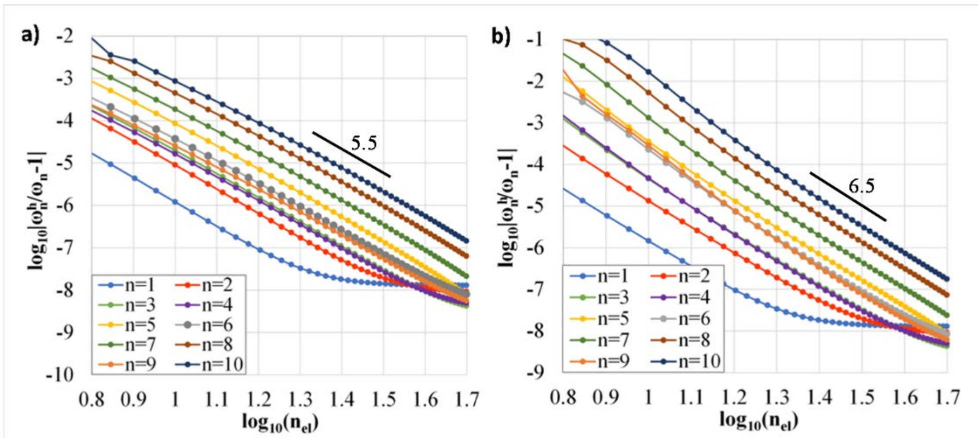

Figure 4. Circular arc, Kh=0.2. Relative error for the lowest 10 eigenfrequencies using the h-refinement with cubic NURBS and: a) C1 continuity; b) C2 continuity (by the authors)

Furthermore, both *p*- and *k*-refinement strategies were investigated. The relative errors of the lowest ten eigenfrequencies are presented in Figure 5, while the errors normalized by the corresponding number of degrees of freedom (n_{DOF}) are shown in Figure 6. The p-refinement strategy is carried out by increasing the polynomial order while keeping both the interelement continuity and the number of elements fixed. It is observed that, for different modes and the selected discretization, different polynomial orders yield the best accuracy. In particular, the quartic polynomial gives the best accuracy for the first mode, the quintic polynomial for the second and fourth modes, and the sextic polynomial for the remaining modes. Figure 5b indicates that increasing interelement continuity does not significantly improve the accuracy, primarily due to the associated reduction in the number of control points and degrees of freedom. However, when normalized by the corresponding number of degrees of freedom, improved performance is observed, as illustrated in Figure 6b. This indicates that increasing interelement continuity leads to higher accuracy per degree of freedom.

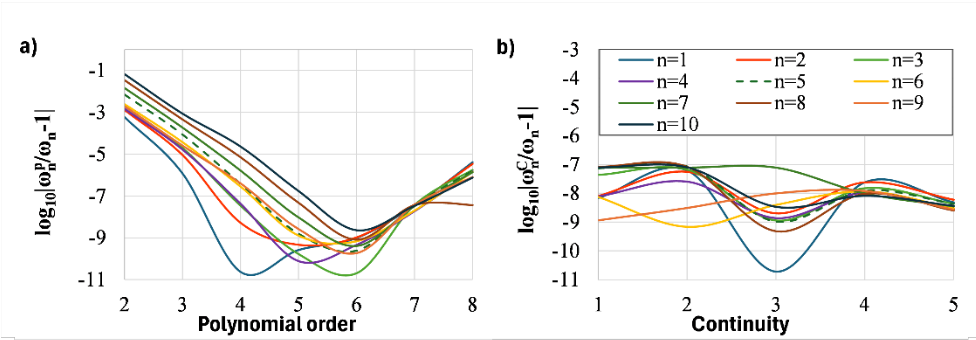

Figure 5. Circular arc, Kh=0.2. Convergence properties for the lowest 10 eigenfrequencies: a) p-refinement with 10 elements and C1 continuity; b) k-refinement with 20 elements and p=6 (diagram by the authors)

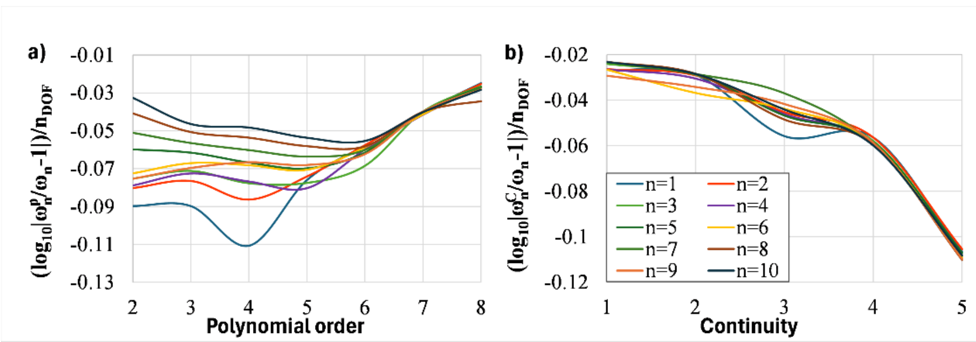

Figure 6. Circular arc, Kh=0.2. Convergence properties for the lowest 10 eigenfrequencies (relative error divided by respective nDOF): a) p-refinement with 10 elements and C1 continuity; b) k-refinement with 20 elements and p=6 (by the authors)

In addition, normalized numerical discrete spectra are evaluated for different interelement continuities (Figure 7). The frequency values are obtained from the model with *N* active degrees of freedom and were normalized by reference frequencies. The reference model was computed using approximately 2000 quartic elements with C^3 interelement continuity, resulting in about 3000 degrees of freedom. A comparison between the lowest and highest continuity levels of the quartic elements also demonstrates the superiority of higher continuity. In this case, variations in *N* did not significantly affect the results.

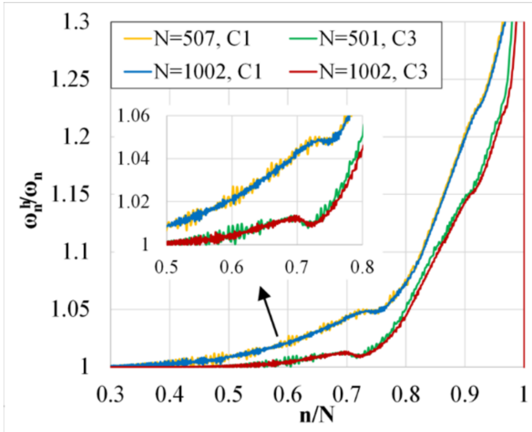

Figure 7. Circular arc, Kh=0.2. The normalized numeric discrete spectra using different continuities (by the authors)

Finally, the mode shapes corresponding to the first ten frequencies for *Kh*=0.2 and the strongly curved model are presented in Figure 8.

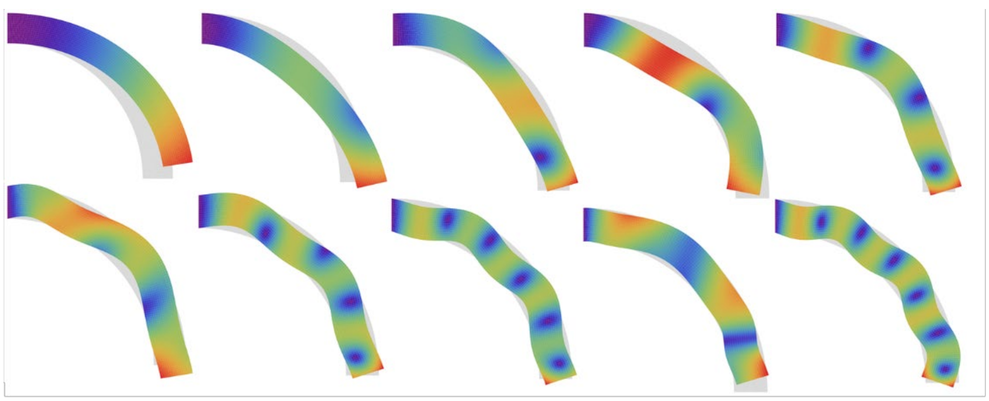

Figure 8. Circular arc, Kh=0.2. First ten mode shapes (by the authors)

5.2. TSCHIRNHAUSEN'S BEAM

This example examines a Tschirnhausen's cubic curve with a rectangular cross-section, whose initial geometry is described exactly by a cubic Bézier curve (Figure 9). The same example was analyzed in [14] using Timoshenko beam theory for different levels of curviness and various boundary conditions, where the initial geometry was not described exactly but was obtained by interpolating a set of points. The material properties of a beam are adopted from the same reference, with *kG*/*E*=0.3.

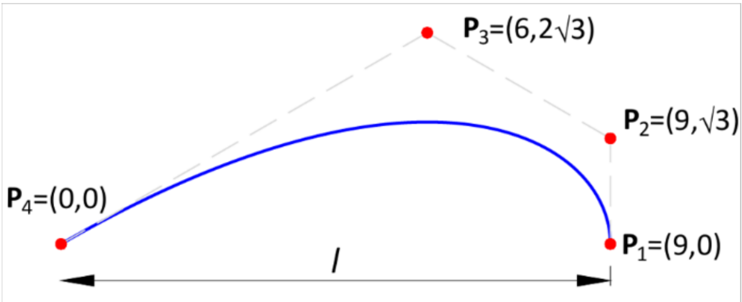

Figure 9. Tschirnhausen's beam (by the authors)

The results are obtained using IGA with 52 quartic elements, C^3 interelement continuity, and 168 degrees of freedom. The frequency values are normalized and expressed as $\bar{\omega}_i = \omega_i l^2/\left(r\sqrt{E/\rho}\right)$, where ω_i denotes the frequency of the i^{th} mode, and l is the beam span.

Comparisons of the lowest six eigenfrequencies for a curviness $K_{max}h$≈0.1 and different boundary conditions are presented in Table 4 and Table 5. For all cases, no noticeable differences are observed between the $IGA\ \bar{D}^0$ and $IGA\ \bar{D}^S$ formulations. The results indicate that for this case, the influence of strong curvature on the constitutive coupling and eigenfrequencies is minimal. When the $IGA\ \bar{D}^S$model is compared with the results reported in [15], the cumulative difference remains moderate. The highest one is observed for the beam clamped at both ends, reaching 5.16%. Furthermore, in comparison with the CPS3 model, the differences remain below 0.5% for most modes. An exception appears in the sixth mode of the hinged-hinged and hinged-clamped configurations, where the differences are approximately 2%. The overall cumulative differences of the two developed formulations are comparable, although the strongly curved formulation consistently achieves a lower total difference.

Table 4. Comparison of the lowest six normalized eigenfrequencies of the Tschirnhausen's beam for $K_{max}h=3\sqrt{3}/50\approx0.1$, IGA formulation

Mode	hinged-hinged		hinged-clamped		clamped-hinged		clamped-clamped	
	$IGA\ \bar{D}^S$	$IGA\ \bar{D}^0$	$IGA\ \bar{D}^S$	$IGA\ \bar{D}^0$	$IGA\ \bar{D}^S$	$IGA\ \bar{D}^0$	$IGA\ \bar{D}^S$	$IGA\ \bar{D}^0$
1	21.11	21.10	26.92	26.91	28.51	28.50	35.48	35.47
2	54.06	54.03	61.75	61.73	64.43	64.39	72.46	72.44
3	104.49	104.43	115.79	115.76	119.22	119.15	131.39	131.35
4	167.50	167.39	179.67	179.61	184.77	184.66	196.72	196.66
5	246.95	246.80	260.12	260.05	268.48	268.30	280.45	280.37
6	304.53	304.53	305.57	305.51	306.34	306.38	310.79	310.75

Table 5. Comparison of the lowest six normalized eigenfrequencies of the Tschirnhausen's beam for $K_{max}h=3\sqrt{3}/50\approx0.1$, reference

Mode	hinged-hinged		hinged-clamped		clamped-hinged		clamped-clamped	
	[15]	Abaqus, CPS3 element	[15]	Abaqus, CPS3 element	[15]	Abaqus, CPS3 element	[15]	Abaqus, CPS3 element
1	21.14	21.15	27.00	26.98	28.58	28.57	35.62	35.57
2	54.22	54.17	62.06	61.91	64.71	64.59	72.93	72.70
3	105.00	104.80	116.70	116.20	120.10	119.60	132.65	131.90
4	168.80	168.00	181.60	180.30	186.60	185.50	199.20	197.70
5	249.70	247.80	263.50	260.60	272.20	269.70	284.20	281.80
6	305.30	296.70	306.80	299.40	306.90	306.30	312.70	311.50

For $K_{max}h\approx0.2$, the influence of curvature becomes more pronounced compared to the previous case (Tables 6–7). While $IGA\ \bar{D}^S$and $IGA\ \bar{D}^0$ models remain in relatively close agreement, the differences are larger than those observed for a smaller level of curviness. The comparison between the $IGA\ \bar{D}^S$ model and the results from [15] shows noticeable differences, with the largest occurring in the sixth mode and reaching 5.69%. The highest cumulative difference of 18% appears in the case where the beam is clamped at both ends. In comparison with the CPS3 isotropic model, the differences remain below 1% for most modes, with the highest being 4.55% in the fourth mode and for the hinged-hinged configuration. The cumulative difference compared to the Abaqus model remains noticeably smaller for the $IGA\ \bar{D}^S$ formulation than for the $IGA\ \bar{D}^0$ formulation. The results are also compared with those from [14], and it is observed that they coincide with the $IGA\ \bar{D}^0$ formulation. The corresponding reference values are listed in Table 8. The first six mode shapes are presented in Figure 10 for the $IGA\ \bar{D}^S$ model and the hinged-hinged configuration.

Table 6. Comparison of the lowest six normalized eigenfrequencies of the Tschirnhausen's beam for $K_{max}h=3\sqrt{3}/25\approx0.2$, IGA formulation

Mode	hinged-hinged		hinged-clamped		clamped-hinged		clamped-clamped	
	$IGA\ \bar{D}^S$	$IGA\ \bar{D}^0$	$IGA\ \bar{D}^S$	$IGA\ \bar{D}^0$	$IGA\ \bar{D}^S$	$IGA\ \bar{D}^0$	$IGA\ \bar{D}^S$	$IGA\ \bar{D}^0$
1	20.99	20.96	26.47	26.45	28.28	28.23	34.79	34.75
2	53.26	53.14	59.67	59.59	63.04	62.91	69.29	69.21
3	102.10	101.88	109.98	109.87	115.91	115.65	123.59	123.46
4	147.53	147.44	147.69	147.56	149.92	149.96	151.83	151.74
5	171.13	171.01	185.98	185.87	185.38	185.09	200.56	200.37
6	237.40	236.83	250.40	250.09	255.40	254.80	267.46	267.16

Table 7. Comparison of the lowest six normalized eigenfrequencies of the Tschirnhausen's beam for $K_{max}h=3\sqrt{3}/25\approx0.2$, reference

Mode	hinged-hinged		hinged-clamped		clamped-hinged		clamped-clamped	
	[15]	Abaqus, CPS3 element	[15]	Abaqus, CPS3 element	[15]	Abaqus, CPS3 element	[15]	Abaqus, CPS3 element
1	21.11	21.02	26.78	26.55	28.54	28.35	35.34	34.94
2	53.87	53.37	60.78	59.87	64.11	63.29	70.95	69.75
3	104.10	102.50	112.90	110.40	119.00	116.60	127.40	124.60
4	148.70	141.10	149.20	142.60	150.70	149.60	153.70	152.30
5	175.10	169.80	192.20	185.20	191.80	187.00	209.40	202.90
6	247.50	238.80	263.30	252.80	268.80	257.70	283.60	271.70

Figure 10. The hinged-hinged Tschirnhausen's beam, $K_{max}h\approx0.2$. First six mode shapes (by the authors)

Table 8. The lowest six normalized eigenfrequencies of the Tschirnhausen's beam for $K_{max}h=3\sqrt{3}/25\approx0.2$, [14]

Mode	hinged-hinged	hinged-clamped	clamped-hinged	clamped-clamped
1	20.96	26.45	28.23	34.75
2	53.14	59.60	62.91	69.21
3	101.88	109.87	115.65	123.46
4	147.44	147.56	149.96	151.74
5	171.01	185.87	185.09	200.37
6	236.83	250.09	254.80	267.16

The convergence analysis is performed for the $IGA\ \bar{D}^S$ model and a beam with $K_{max}h\approx0.1$, hinged at both ends. The *h*-refinement strategy is done using cubic NURBS with two different interelement continuities (Figure 11). The results indicate good convergence characteristics, similar to the previous example.

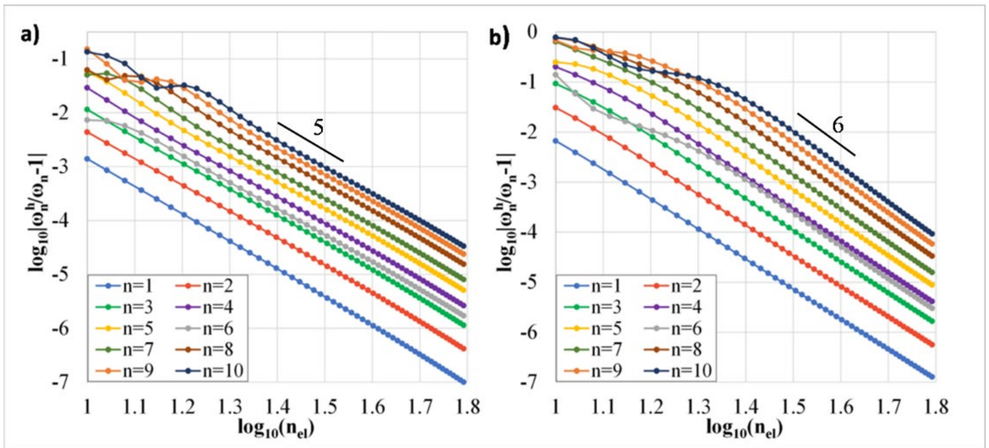

Figure 11. Tschirnhausen's beam, Kmaxh≈0.1. Relative error for the lowest 10 eigenfrequencies using the h-refinement with cubic NURBS and: a) C1 continuity; b) C2 continuity (by the authors)

In the case of *p*-refinement (Figures 12a and 13a), local error minima are again observed, indicating that there is a preferable polynomial order for a chosen discretization. For the adopted mesh consisting of 20 elements with C^1 interelement continuity, a particularly pronounced minimum appears in the second mode at polynomial order *p*=6. This order provides the best accuracy also for the second mode, whereas higher modes achieve better accuracy with septic elements. The *k*-refinement analysis is performed using a mesh of 40 sextic elements, as shown in Figures 12b and 13b. Higher interelement continuity again demonstrates improved accuracy per degree of freedom. However, when the relative error is considered without normalization by the number of degrees of freedom, a reduction in accuracy is observed only for the highest continuity levels. This behavior can be attributed to the sufficiently dense discretization, where the reduced number of control points may influence the resolution of higher modes. Notably, for the ninth mode, C^3 continuity yields the best performance despite the reduced number of control points.

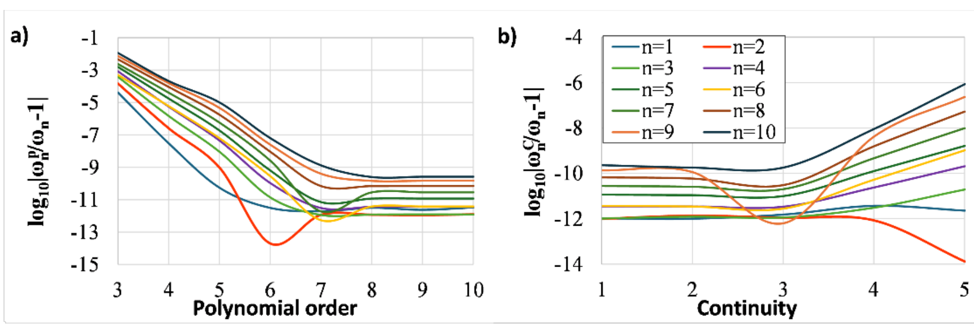

Figure 12. Tschirnhausen's beam, $K_{max}h$≈0.1. Convergence properties for the lowest 10 eigenfrequencies: a) p-refinement with 20 elements and C1 continuity; b) k-refinement with 40 elements and p=6 (by the authors)

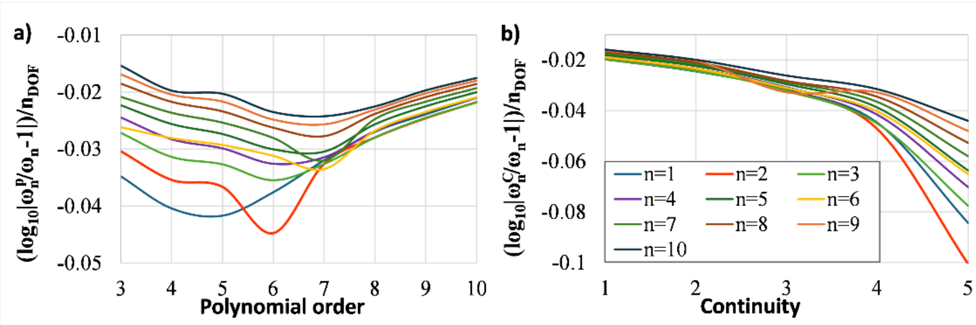

Figure 13. Tschirnhausen's beam, $K_{max}h$≈0.1. Convergence properties for the lowest 10 eigenfrequencies (relative error divided by respective nDOF): a) p-refinement with 20 elements and C1 continuity; b) k-refinement with 40 elements and p=6 (by the authors)

In the present case, the Jacobian of the curve varies gradually and, therefore, the parameterization can be considered weakly nonlinear. This issue can be addressed using the reparameterization technique proposed in [19].

6. CONCLUSIONS

Isogeometric analysis enables the exact representation of the initial geometry using NURBS, which represent a general case of spline-based geometry description. In this work, an isogeometric formulation for the free vibration analysis of arbitrarily curved planar beams, based on the geometrically consistent Timoshenko beam theory, has been developed. The formulation is implemented in a curvilinear coordinate system and involves the effect of initial curvature. A detailed investigation of selected numerical examples has demonstrated the suitability and robustness of the proposed isogeometric approach, confirming its validity even for strongly curved beams. The curviness level strongly influences the choice of an appropriate beam theory. In particular, shear deformation must be included for moderately thick beams, and coupling constitutive effects must be properly accounted for when analysing strongly curved beams. These coupling effects are expected to be more emphasized in spatial beams, nonlinear analysis, and finite strain theory.

The convergence study generally indicates that higher interelement continuity leads to improved accuracy per number of degrees of freedom. The same conclusion is supported by the analysis of the normalized numerical discrete spectra. However, regarding the k-refinement and adopted discretizations, improved accuracy was occasionally achieved for specific modes with lower levels of interelement continuity. The p-refinement strategy revealed the presence of local minima, indicating that, for certain vibration modes and the adopted discretization, there exist preferable polynomial degrees. Future research will be directed towards more complex dynamic problems.

7. ACKNOWLEDGMENT

This research was partly funded by the Austrian Science Fund (FWF) 10.55776/P36019. For the purpose of open access, the authors have applied a CC BY public copyright licence to any Author Accepted Manuscript version arising from this submission.

8. REFERENCES

[1] T. J. R. Hughes, J. A. Cottrell, and Y. Bazilevs, "Isogeometric analysis: CAD, finite elements, NURBS, exact geometry and mesh refinement," *Computer Methods in Applied Mechanics and Engineering*, vol. 194, no. 39–41, pp. 4135–4195, 2005. DOI: https://doi.org/10.1016/j.cma.2004.10.008

[2] A. Reali, "An isogeometric analysis approach for the study of structural vibrations," *Journal of Earthquake Engineering*, vol. 10, no. 1, pp. 1–30, 2006. DOI: https://doi.org/10.1080/13632460609350626

[3] J. A. Cottrell, A. Reali, Y. Bazilevs, and T. J. R. Hughes, "Isogeometric analysis of structural vibrations," *Computer Methods in Applied Mechanics and Engineering*, vol. 195, no. 41–43, pp. 5257–5296, 2006. DOI: https://doi.org/10.1016/j.cma.2005.09.027

[4] L. Greco and M. Cuomo, "B-Spline interpolation of Kirchhoff-Love space rods," *Computer Methods in Applied Mechanics and Engineering*, vol. 256, pp. 251–269, 2013. DOI: https://doi.org/10.1016/j.cma.2012.11.017

[5] A. Borković, S. Kovačević, G. Radenković, S. Milovanović, and M. Guzijan-Dilber, "Rotation-free isogeometric analysis of an arbitrarily curved plane Bernoulli-Euler beam," *Computer Methods in Applied Mechanics and Engineering*, vol. 334, pp. 238–267, 2018. DOI: https://doi.org/10.1016/j.cma.2018.02.002

[6] D. Vo and P. Nanakorn, "A total Lagrangian Timoshenko beam formulation for geometrically nonlinear isogeometric analysis of planar curved beams," *Acta Mechanica*, vol. 231, no. 9, pp. 2827–2847, 2020. DOI: https://doi.org/10.1007/s00707-020-02675-x

[7] R. Echter and M. Bischoff, "Numerical efficiency, locking and unlocking of NURBS finite elements," *Computer Methods in Applied Mechanics and Engineering*, vol. 199, no. 5–8, pp. 374–382, 2010. DOI: https://doi.org/10.1016/j.cma.2009.02.035

[8] L. Beirão da Veiga, C. Lovadina, and A. Reali, "Avoiding shear locking for the Timoshenko beam problem via isogeometric collocation methods," *Computer Methods in Applied Mechanics and Engineering*, vol. 241–244, pp. 38–51, 2012. DOI: https://doi.org/10.1016/j.cma.2012.05.020

[9] F. Auricchio, L. Beirão da Veiga, J. Kiendl, C. Lovadina, and A. Reali, "Locking-free isogeometric collocation methods for spatial Timoshenko rods," *Computer Methods in Applied Mechanics and Engineering*, vol. 263, pp. 113–126, 2013. DOI: https://doi.org/10.1016/j.cma.2013.03.009

[10] R. Bouclier, T. Elguedj, and A. Combescure, "Locking free isogeometric formulations of curved thick beams," *Computer Methods in Applied Mechanics and Engineering*, vol. 245–246, pp. 144–162, 2012. DOI: https://doi.org/10.1016/j.cma.2012.06.008

[11] J. Kiendl, F. Auricchio, and A. Reali, "A displacement-free formulation for the Timoshenko beam problem and a corresponding isogeometric collocation approach," *Meccanica*, vol. 53, no. 6, pp. 1403–1413, 2018. DOI: https://doi.org/10.1007/s11012-017-0745-7

[12] Z. Sun, D. Wang, and W. Gao, "An equal-order strain projection formulation for locking-free isogeometric analysis of shear deformable curved beams," *Engineering Structures*, vol. 335, 2025, Art. no. 120312. DOI: https://doi.org/10.1016/j.engstruct.2025.120312

[13] O. Weeger, U. Wever, and B. Simeon, "Isogeometric analysis of nonlinear Euler-Bernoulli beam vibrations," *Nonlinear Dynamics*, vol. 72, no. 4, pp. 813–835, 2013. DOI: https://doi.org/10.1007/s11071-013-0755-5

[14] A.-T. Luu, N.-I. Kim, and J. Lee, “Isogeometric vibration analysis of free-form Timoshenko curved beams,” *Meccanica*, vol. 50, no. 1, pp. 169–187, 2015. DOI: https://doi.org/10.1007/s11012-014-0062-3

[15] A. Borković, S. Kovačević, G. Radenković, S. Milovanović, and D. Majstorović, “Rotation-free isogeometric dynamic analysis of an arbitrarily curved plane Bernoulli-Euler beam,” *Engineering Structures*, vol. 181, pp. 192–215, 2019. DOI: https://doi.org/10.1016/j.engstruct.2018.12.003

[16] D. Wang, W. Liu, and G. Zhang, “Novel higher order matrices for isogeometric structural vibration,” *Computer Methods in Applied Mechanics and Engineering*, vol. 260, pp. 92–108, 2013. DOI: https://doi.org/10.1016/j.cma.2013.03.011

[17] A.-T. Luu, N.-I. Kim, and J. Lee, “NURBS-based isogeometric vibration analysis of generally laminated deep curved beams with variable curvature,” *Composite Structures*, vol. 119, pp. 150–165, 2015. DOI: https://doi.org/10.1016/j.compstruct.2014.08.014

[18] H. Liu, X. Zhu, and D. Yang, “Isogeometric method based in-plane and out-of-plane free vibration analysis for Timoshenko curved beams,” *Structural Engineering and Mechanics*, vol. 59, no. 3, pp. 503–526, 2016. DOI: https://doi.org/10.12989/sem.2016.59.3.503

[19] S. Hosseini, A. Hashemian, and A. Reali, “On the application of curve reparameterization in isogeometric vibration analysis of free-form curved beams,” *Computers & Structures*, vol. 209, pp. 117–129, 2018. DOI: https://doi.org/10.1016/j.compstruc.2018.08.009

[20] H. Liu, D. Yang, X. Wang, Y. Wang, L. Chen, and Z.-P. Wang, “Smooth size design for the natural frequencies of curved Timoshenko beams using isogeometric analysis,” *Structural and Multidisciplinary Optimization*, vol. 59, no. 4, pp. 1143–1162, 2019. DOI: https://doi.org/10.1007/s00158-018-2119-8

[21] Z. Kheladi, S. M. Hamza-Cherif, and M. E. A. Ghernaout, “Free vibration analysis of variable stiffness laminated composite beams,” *Mechanics of Advanced Materials and Structures*, vol. 28, no. 18, pp. 1889–1916, 2021. DOI: https://doi.org/10.1080/15376494.2020.1712750

[22] L. Greco, D. Castello, A. Cammarata, and M. Cuomo, “Spherical B-spline interpolation with application to a mixed isogeometric Cosserat rod formulation,” *Computer Methods in Applied Mechanics and Engineering*, vol. 446, 2025, Art. no. 118239. DOI: https://doi.org/10.1016/j.cma.2025.118239

[23] E. Tufekci and A. Arpaci, “Exact solution of in-plane vibrations of circular arches with account taken of axial extension, transverse shear and rotatory inertia effects,” *Journal of Sound and Vibration*, vol. 209, no. 5, pp. 845–856, 1998. DOI: https://doi.org/10.1006/jsvi.1997.1290

[24] L. Piegl and W. Tiller, *The NURBS Book*, 2nd ed., Berlin, Heidelberg, Germany: Springer, 1997. DOI: https://doi.org/10.1007/978-3-642-59223-2

[25] J. A. Cottrell, T. J. R. Hughes, and Y. Bazilevs, *Isogeometric analysis: Towards Integration of CAD and FEA*, Chichester, U.K.: John Wiley & Sons, 2009. DOI: https://doi.org/10.1002/9780470749081

[26] G. Radenković, *Isogeometric theory of structures*, Belgrade, Serbia: Faculty of Architecture (in Serbian), 2014.

[27] G. Radenković, *Finite rotation and finite strain isogeometric structural analysis*, Belgrade, Serbia: Faculty of Architecture (in Serbian), 2017.

AUTHORS' BIOGRAPHIES

Snježana Milovanović

Snježana Milovanović is a senior assistant at the University of Banja Luka. She obtained her bachelor's and master's degrees at the Faculty of Architecture, Civil Engineering and Geodesy in Banja Luka as the best graduate student. She is a PhD candidate at the Faculty of Architecture, Civil Engineering and Geodesy in Banja Luka. The main subject of her research is computational models for the analysis of beams and shells.

Aleksandar Borković

Aleksandar Borković is a researcher at TU Graz and an associate professor at the University of Banja Luka. His research focus is on computational modeling of interactions between beams and shells and experimental investigations of structural response. He collaborates internationally and is involved in academic teaching and research projects in engineering mechanics and computational modeling.

Dijana Tatar

Dijana Tatar is a senior teaching assistant at the University of Banja Luka. She is a doctoral candidate at the Faculty of Architecture, Civil Engineering and Geodesy in Banja Luka, currently in the thesis preparation phase. Her primary research interest lies in computational modeling of beams and shells.

Ognjen Mijatović

Ognjen Mijatović is an associate professor at the University of Banja Luka. He received his undergraduate degree from the same faculty and completed his master's and doctoral studies in structural engineering at the Faculty of Civil Engineering, University of Belgrade. His research focuses on structural dynamics, contact mechanics, frictional damping, and the influence of surface roughness on structural response. He is a member of the International Committee on Joint Mechanics and collaborates with researchers from institutions including Sandia National Laboratories and Tianjin Chengjian University. In addition to his academic work, he has professional experience in structural design and supervision on international projects in the United Arab Emirates, Azerbaijan, and Bahrain, including high-rise towers and large-span steel structures.

ИЗОГЕОМЕТРИЈСКА АНАЛИЗА СЛОБОДНИХ ВИБРАЦИЈА ТИМОШЕНКОВЕ ГРЕДЕ У РАВНИ

Сажетак: Овај рад представља изогеометријску формулацију за линеарну анализу сопствених вибрација произвољно закривљених Тимошенкових греда у равни. Модел је развијен кориштењем криволинијских координата, чиме се обезбеђује конзистентан кинематички опис и тачна репрезентација снажно закривљених геометрија. Геометрија греде је тачно описана примјеном Б-Сплајн и НУРБС базних функција у оквиру изогеометријске анализе, док се исте функције користе за апроксимацију кинематичког поља. Спроведена је детаљна нумеричка анализа у циљу процјене својстава конвергенције и тачности предложене формулације. Својства конвергенције испитана су примјеном h-, p- и k- побољшања мреже коначних елемената. Добијени резултати показују добра конвергенцијска својства, при чему се већа тачност може постићи уз мањи број степена слободе када се примјењује виши континуитет на границама елемената. Предложена формулација представља тачан и ефикасан приступ за анализу вибрација закривљених гредних структура и пружа поуздану основу за даља проширења на сложеније конструктивне и динамичке проблеме.

Кључне ријечи: Тимошенкова греда, произвољно закривљена греда, слободне вибрације, ИГА, НУРБС